

3-1-2022

Nonlinear dynamics of the non-Hermitian Su-Schrieffer-Heeger model

Pieter M. Gunnink
Universiteit Utrecht

Benedetta Flebus
Boston College

Hilary M. Hurst
San Jose State University, hilary.hurst@sjsu.edu

Rembert A. Duine
Universiteit Utrecht

Follow this and additional works at: https://scholarworks.sjsu.edu/faculty_rsca

Recommended Citation

Pieter M. Gunnink, Benedetta Flebus, Hilary M. Hurst, and Rembert A. Duine. "Nonlinear dynamics of the non-Hermitian Su-Schrieffer-Heeger model" *Physical Review B* (2022). <https://doi.org/10.1103/PhysRevB.105.104433>

This Article is brought to you for free and open access by SJSU ScholarWorks. It has been accepted for inclusion in Faculty Research, Scholarly, and Creative Activity by an authorized administrator of SJSU ScholarWorks. For more information, please contact scholarworks@sjsu.edu.

Nonlinear dynamics of the non-Hermitian Su-Schrieffer-Heeger modelPieter M. Gunnink^{1,*}, Benedetta Flebus², Hilary M. Hurst³, and Rembert A. Duine^{1,4}¹*Institute for Theoretical Physics and Center for Extreme Matter and Emergent Phenomena, Utrecht University, Leuvenlaan 4, 3584 CE Utrecht, The Netherlands*²*Department of Physics, Boston College, 140 Commonwealth Avenue, Chestnut Hill, Massachusetts 02467, USA*³*Department of Physics and Astronomy, San José State University, San José, California 95192, USA*⁴*Department of Applied Physics, Eindhoven University of Technology, P.O. Box 513, 5600 MB Eindhoven, The Netherlands*

(Received 21 January 2022; revised 21 March 2022; accepted 22 March 2022; published 29 March 2022)

We numerically determine the robustness of the lasing edge modes in a spin-torque oscillator array that realizes the non-Hermitian Su-Schrieffer-Heeger model. Previous studies found that the linearized dynamics can enter a topological regime in which the edge mode is driven into auto-oscillation, while the bulk dynamics are suppressed. Here we investigate the full nonlinear and finite-temperature dynamics, whose understanding is essential for spin-torque oscillators-based applications. Our analysis shows that the lasing edge mode dynamics persist in the nonlinear domain for a broad range of parameters and temperatures. We investigate the effects of perturbations relevant to experimental implementations and discuss which ones might be detrimental to the stability of the lasing edge mode. Finally, we map our model onto a photonic model. Our analysis has the potential to shed light onto the dynamics of a plethora of non-Hermitian systems with nonlinearities.

DOI: [10.1103/PhysRevB.105.104433](https://doi.org/10.1103/PhysRevB.105.104433)**I. INTRODUCTION**

The application of topology to condensed matter systems has been profoundly fruitful on both theoretical and experimental fronts and has led to the discovery of a wide range of new phenomena and materials [1]. Recently, considerable effort has been devoted towards the exploration of non-Hermitian systems [2,3] with active gain and loss. A framework for addressing non-Hermitian topological phases has been provided by the growing field of topological theories of non-Hermitian systems [4–7].

Recent studies have shown that the bulk-boundary correspondence [8], which is the cornerstone of topology in Hermitian systems, also holds for specific non-Hermitian systems [9], although not in general [10–12]. Some systems also exhibit a non-Hermitian skin effect, where even the bulk modes can be very sensitive to boundary conditions [13]. Nevertheless, the existence of non-Hermitian edge modes has been shown in a variety of systems, such as microring resonators [14–16] and electrical circuits [17–19].

One of the most striking properties of non-Hermitian topological phases is the coexistence of lasing edge modes, i.e., edge states with gain-like dynamics, with a purely real bulk spectrum. Most importantly, these modes are topologically protected [5] and can therefore be useful in applications, since they are robust against disorder. In photonics these lasing modes have been used to build a single-mode laser stable against perturbations [20].

The majority of developments in non-Hermitian topological insulators have been in the field of photonics [21–24],

where gain and dissipation can be readily tuned. Recent works have also unveiled non-Hermitian topological phases in mechanical [25,26], electrical [17–19,27], and magnetic systems [28–30]. Here we focus on magnetic systems, in which the loss is inherently present due to coupling of the magnonic excitations to the lattice and whose dynamics can be driven using spin-transfer torques. Due to the tunability of gain and loss, magnetic systems might represent a nearly ideal system to explore non-Hermitian phenomena.

Specifically, we consider the topology of the one-dimensional (1D) array of spin-torque oscillators (STOs) as shown in Fig. 1, building on the work of Flebus *et al.* [31]. Spin-torque oscillators are current-driven magnetic nanoparticles, whose magnetization dynamics are determined by the balance of spin current injection and intrinsic (Gilbert-like) dissipation [32]. It has been experimentally shown that the coupling between STOs arranged in an array can be tuned [33,34]. Flebus *et al.* [31] have shown that, by modulating the coupling between STOs and the local spin injection, the array can be driven into the topological phase of the non-Hermitian Su-Schrieffer-Heeger (SSH) model [35], known to host lasing edge states [36,37]. However, STOs also exhibit strong nonlinear effects, such as a nonlinear frequency shift [32]. Furthermore, thermal fluctuations have also been shown to introduce significant noise into these systems [38]. In this paper, we aim to investigate in detail how nonlinearities and thermal fluctuations affect the topological character of a 1D array of STOs, in order to assess the experimental feasibility of this setup. Our results can be straightforwardly generalized to the realization of this model in photonic systems, which also exhibit nonlinear and stochastic dynamics, making our paper of interest to a broader audience.

*p.m.gunnink@uu.nl

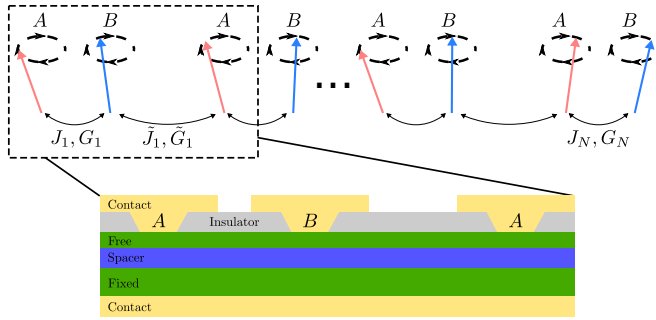


FIG. 1. Schematic illustration of the model considered in this paper. The array of STOs is represented as a 1D lattice with a two-sublattice (A and B) unit cell. The STOs are connected via a metallic spacer that mediates an intracell (J_i, G_i) and intercell (\tilde{J}_i, \tilde{G}_i) complex nearest-neighbor hopping. The inset shows a possible experimental realization of the STOs array, with the stacking of contact|fixed layer|spacer|free layer|contact. The magnetic layers extend throughout the array, and spin waves excited by one STO can reach and dissipatively couple the neighboring STOs.

This paper is organized as follows: In Sec. II we start by introducing our model and we analyze its topological properties. In Sec. III, we discuss in detail the numerical simulations deployed to investigate the nonlinear dynamics at finite temperatures. We present the results of our simulations for a wide range of parameters in Sec. IV and we identify the parameter regions where the lasing edge mode is realized. In Sec. V we show how our model is similar to previous implementations of the non-Hermitian SSH model in photonic systems. A summary and conclusions are given in Sec. VI. Finally, we discuss the details of our numerical and analytical calculations in, respectively, Appendix A and B.

II. SYSTEM

We consider an array of $2N$ STOs that realize the non-Hermitian SSH model, as shown in Fig. 1. A STO consists of a magnetic polarizing layer separated from a magnetic free layer by a thin spacer. An external magnetic field $\mathbf{H} = H_0 \hat{z}$ sets the equilibrium direction of the magnetic order parameter \mathbf{m} of the free layer. The polarizing layer converts a DC current into a spin current J_s , which, in turn, exerts a spin-transfer torque on the magnetic order parameter \mathbf{m} . The loss and gain dynamics of the ferromagnetic order parameter \mathbf{m} associated with each nanopillar is described by the Landau-Lifshitz-Gilbert (LLG) equation as [32]

$$\begin{aligned} \partial_t \mathbf{m}_{\eta,i}|_0 &= \omega_{\eta,i} \hat{z} \times \mathbf{m}_{\eta,i} + \alpha_{\eta,i} \mathbf{m}_{\eta,i} \times \partial_t \mathbf{m}_{\eta,i} \\ &+ J_{s\eta,i} \mathbf{m}_{\eta,i} \times (\mathbf{m}_{\eta,i} \times \hat{z}), \end{aligned} \quad (1)$$

where i labels the unit cells and $\eta = A, B$. Here, $\omega_{\eta,i} = \gamma_{\eta,i}(H_0 - 4\pi m_{z,\eta,i})$ is the ferromagnetic resonance frequency, $\gamma_{\eta,i}$ is the gyromagnetic ratio, and $M_{\eta,i}$ the saturation magnetization. $\alpha_{\eta,i} \ll 1$ is the Gilbert damping parameter that captures the relaxation of the macrospin Kittel mode. The last term is the spin-transfer torque exerted by the spin current $J_{s\eta,i}$ on the magnetic order parameter.

We consider three kinds of intra (inter)-cell couplings between the STOs. Firstly, we account for the Ruderman-

Kittel-Kasuya-Yosida (RKKY)-type exchange, parameterized by the frequencies J_i (\tilde{J}_i). Secondly, there is a dissipative coupling G_i (\tilde{G}_i), which is mediated by spin pumping through the spacer layers [39]. The exchange and dissipative couplings only couple the nearest neighbors, as indicated in Fig. 1. These two couplings were already introduced in Ref. [31]. Additionally, in this paper we also introduce the dipolar couplings between the STOs, which affect the nonlinear dynamics [40,43].

The dynamics of the coupled array are then described by

$$\begin{aligned} \partial_t \mathbf{m}_{A,i}|_{\text{coup}} &= -\mathbf{m}_{A,i} \times (J_i \mathbf{m}_{B,i} + \tilde{J}_{i-1} \mathbf{m}_{B,i-1}) \\ &- G_i \mathbf{m}_{B,i} \times \partial_t \mathbf{m}_{B,i} - \tilde{G}_{i-1} \mathbf{m}_{B,i-1} \times \partial_t \mathbf{m}_{B,i-1} \\ &- \Omega_d \mathbf{m}_{A,i} \times \sum'_{\eta,j} \frac{3\hat{\mathbf{x}}(\hat{\mathbf{x}} \cdot \mathbf{m}_{\eta,j}) - \mathbf{m}_{\eta,j}}{r_{A\eta,ij}^3}, \end{aligned} \quad (2)$$

$$\begin{aligned} \partial_t \mathbf{m}_{B,i}|_{\text{coup}} &= -\mathbf{m}_{B,i} \times (J_i \mathbf{m}_{A,i} + \tilde{J}_i \mathbf{m}_{A,i+1}) \\ &- G_i \mathbf{m}_{A,i} \times \partial_t \mathbf{m}_{A,i} - \tilde{G}_i \mathbf{m}_{A,i+1} \times \partial_t \mathbf{m}_{A,i+1} \\ &- \Omega_d \mathbf{m}_{B,i} \times \sum'_{\eta,j} \frac{3\hat{\mathbf{x}}(\hat{\mathbf{x}} \cdot \mathbf{m}_{\eta,j}) - \mathbf{m}_{\eta,j}}{r_{B\eta,ij}^3}, \end{aligned} \quad (3)$$

where \sum' indicates that the sum excludes the self-interaction. The dipolar interaction is parametrized by $\Omega_d = \gamma_{\eta,i} V_{\text{eff}\eta,i} / a^3$, where $V_{\text{eff}\eta,i}$ is the effective volume of a STO and a is the separation distance between STOs, which we assume to be constant. $r_{\eta\eta',ij} = R_{\eta\eta',ij} / a$ is the normalized distance between $\text{STO}_{\eta i}$ and $\text{STO}_{\eta' j}$. Here we have incorporated terms proportional to the Gilbert-like on-site damping of the G_i, \tilde{G}_i couplings into the Gilbert damping, i.e., $\alpha_{A,i} = \alpha_{\eta,i} + G_i + \tilde{G}_i$ and $\alpha_{B,i} = \alpha_{\eta,i} + G_i + \tilde{G}_{i-1}$. In what follows we assume identical unit cells and drop the dependency on the unit cell index i , unless stated otherwise, such that $\omega_{\eta,i} = \omega$, $\alpha_{\eta,i} = \alpha + G + \tilde{G}$, $J_i = J$, $\tilde{J}_i = \tilde{J}$, $G_i = G$ and $\tilde{G}_i = \tilde{G}$. Furthermore, we assume spin-current injection only on sublattice A, i.e., $J_{s,B} = 0$, $J_{s,A} = J_s$.

The equations of motion for this system are then given by Eqs. (1)–(3), which can be linearized around the equilibrium direction of the magnetic order parameter. We write $\mathbf{m}_{\eta,i} = (m_{\eta,i}^x, m_{\eta,i}^y, 1)$ and neglect terms that are second order in the fluctuations from equilibrium. We then introduce the complex variable $2m_{\eta,i} = m_{\eta,i}^x - im_{\eta,i}^y$ and invoke the Holstein-Primakoff transformation [44] $m_{\eta,i}(t) = \langle \eta_i \rangle e^{-i\omega t}$, where $\eta_i = a_i, b_i$ are second-quantized operators annihilating magnons at sublattice η and obeying bosonic commutation relations. From the corresponding Heisenberg equation of motion we can identify the effective quadratic magnon Hamiltonian, which we will use next for topological classification.

The nonlinear character of the equations of motion means that the Hamiltonian should also contain higher order interactions. The on-site dynamics, i.e., Eq. (1), would introduce on-site interaction terms, and the exchange interaction would result in quartic and higher order interactions terms between neighboring spins. How these interaction terms affect the topology is still an unanswered question [41,42]. We therefore only consider the quadratic Hamiltonian to determine the topological properties. However, in our numerical simulations

we do take into account the nonlinearities of the equations of motion, thus capturing the full dynamics resulting from the higher order interaction terms.

Our starting point is the \mathcal{PT} (parity-time) symmetric case, analyzed as well by Flebus *et al.* [31]. Here $J_s = 2\alpha\omega$ and $\Omega_d = G = \tilde{G} = 0$. In this regime, the system hosts two edge modes with energies $\text{Re } E - \omega = 0$ and $\text{Im } E \neq 0$ for $|J| < |\tilde{J}|$. The \mathcal{PT} symmetry indicates the system is invariant under combined parity (swapping site A with B and vice versa) and time reversal ($t \rightarrow -t$) operations [2,3]. We assume the strength of the dissipative coupling and the dipole-dipole interactions to be small compared to ω , and treat them as perturbations. We note here that we do have access to the full (including nonlinear) dynamics that result from the dissipative and dipolar coupling and only treat them as perturbations in the topological analysis. In the simulations that follow we describe the full dynamics of the system, including dissipative and dipolar couplings.

The Hamiltonian of the \mathcal{PT} -symmetric model is

$$\begin{aligned} H_i &= \omega[a_i^\dagger a_i + b_i^\dagger b_i] + i(J_{sA} - \alpha\omega)a_i^\dagger a_i \\ &\quad - i\alpha\omega b_i^\dagger b_i - J[a_i^\dagger b_i + \text{H.c.}] \\ &\quad - \tilde{J}[a_i^\dagger b_{i-1} + \text{H.c.}], \end{aligned} \quad (4)$$

for $i \neq 1, N$, with open boundary conditions

$$\begin{aligned} H_j &= \omega[a_j^\dagger a_j + b_j^\dagger b_j] + i(J_{sA} - \alpha\omega)a_j^\dagger a_j \\ &\quad - i\alpha\omega b_j^\dagger b_j - J[a_j^\dagger b_j + \text{H.c.}] \\ &\quad - \tilde{J}[b_j^\dagger a_l + \text{H.c.}], \end{aligned} \quad (5)$$

where $j = 1, N$ and $l = 2, N - 1$. The full Hamiltonian, including the dissipative and dipole-dipole coupling, is given in Appendix B.

We first briefly discuss the phase diagram, which captures the linear dynamics. For a full discussion the reader is referred to the earlier work of Flebus *et al.* [31]. The topological nature of the edge modes can be characterized by a global complex Berry phase [36], i.e., an integer that predicts the number of pairs of edge modes. The complex Berry phase can be found to be one for $|J| < |\tilde{J}|$, signaling the presence of topologically protected edge states.

Furthermore, the system has an exceptional point at $|\tilde{J} \pm \alpha\omega| = |J|$, where the system transitions from the \mathcal{PT} -unbroken into the \mathcal{PT} -broken regime [36]. In the \mathcal{PT} -unbroken regime the edge state spectra come as complex-conjugated pairs, while the bulk spectrum is purely real. Thus, the edge mode with positive imaginary energy starts lasing, while the bulk modes remain inactive. In the \mathcal{PT} -broken regime the bulk modes also become complex valued, such that they also will start lasing spontaneously. In order to isolate the dynamics of the lasing edge mode we therefore require $|J| < |\tilde{J} - \alpha\omega|$, i.e., to be in the \mathcal{PT} -unbroken regime.

When dissipative couplings G, \tilde{G} are present, all bulk modes will have a nonzero imaginary component, since the system is no longer \mathcal{PT} symmetric. The edge mode is still well defined and separated in energy from the bulk modes. However, because all bulk modes have a nonzero imaginary component, these modes can start lasing as well, as was also noted by Flebus *et al.* [31]. We note that chiral-inversion (CI)

symmetry protects the stability of the edge states [45], such that the topologically protected edge modes are now present for $|J - i\tilde{G}\omega| < |\tilde{J} - i\tilde{G}\omega|$. Since in almost all experimental realizations of the setup discussed here the dissipative coupling will be much weaker than the RKKY-type coupling, the system will most likely still be in the topologically nontrivial regime.

For the dipole-dipole interactions we note that the dipolar fields are \mathcal{PT} invariant, and thus the bulk spectrum will remain real. However, long-range interactions are typically not captured by topological classifications [46], and it is unclear from the linearized model alone how the long-range dipolar interaction will affect the lasing edge modes. This will be investigated numerically in the next section.

As was noted before, the phase diagram only captures the linear behavior of the STO array. In the STO array considered here, the STOs are easily driven into the nonlinear regime [31,47]. Nonlinearities therefore need to be taken into account when describing this topological array. Thus, we proceed to investigate the full nonlinear dynamics numerically.

III. SIMULATIONS

We numerically simulate the system described by Eqs. (1)–(3), using the parametrization outlined in Appendix A. This parametrization maps the magnetic order parameter $m_{\eta,i}$ to the microwave power $p_{\eta,i}$ (which is experimentally measurable) and the azimuthal angle $\phi_{\eta,i}$. The thermal fluctuations are taken into account by using a stochastic field, the strength of which is chosen such that an isolated STO reaches thermal equilibrium [38]. We note that this noise will equilibrate the whole array to $2N$ individual STOs in thermal equilibrium, since the couplings between STOs are not taken into account in the equilibration. However, we assume couplings to be weak compared to the on-site dynamics (i.e., $J, \tilde{J} \ll \omega$), making this a valid approximation. The noise is thus chosen to have zero mean and a second-order correlator

$$\begin{aligned} \langle f_{\eta,i}(t) f_{\eta',j}(t') \rangle &= 0; \quad \langle f_{\eta,i}(t) f_{\eta',j}^*(t') \rangle \\ &= 2\delta_{i,j} \delta_{\eta,\eta'} D_{\eta,i}(p_{\eta,i}) \delta(t - t'), \end{aligned} \quad (6)$$

where $D_{\eta,i}(p)$ is a diffusion coefficient that characterizes the noise amplitude, which has to be taken to be dependent on $p_{\eta,i}$ in order to correctly describe the stochastic dynamics of a nonlinear oscillator. The explicit form of $D_{\eta,i}(p)$ is reported in Appendix A.

In order to integrate the resulting stochastic differential equation we use the Euler-Heun algorithm as implemented in the DifferentialEquations.jl package [48]. As initial conditions we take the phase $\phi_{\eta,i}$ to be uniformly and randomly distributed between 0 and 2π and the power $p_{\eta,i}$ to be distributed according to the equilibrium Boltzmann distribution

$$P_{eq} \propto \exp\left[-\frac{2\lambda_{\eta,i}}{k_B T} p_{\eta,i}\right], \quad (7)$$

where $\lambda_{\eta,i}$ is a scale factor relating the dimensionless oscillator power p and the oscillator energy.

Since this system is inherently stochastic, both from the initial conditions and the thermal fluctuations, we collect

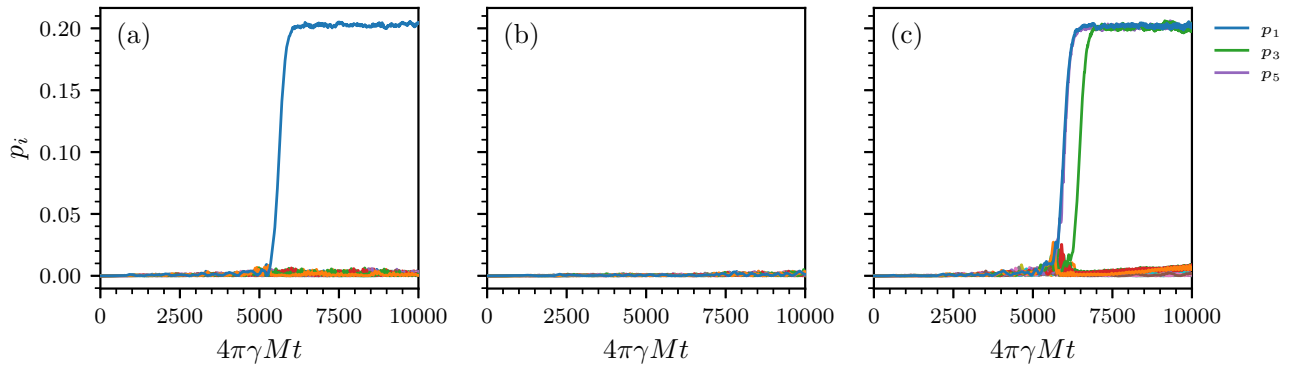


FIG. 2. Three types of behavior of the system, with $\tilde{J} = -0.025/4\pi\gamma M$, $J/\tilde{J} = 0.5$, $k_B T/\lambda = 10^{-5}$, and $G = \Omega_d = 0$. (a) Only the edge mode starts lasing, while all the bulk modes are suppressed. (b) No modes start lasing within the specified time frame. (c) Both the edge modes and bulk modes start lasing. The simulation is run for $4\pi\gamma M t = 10^5$, which for a typical STO with $4\pi\gamma M = 10$ GHz is equal to $10 \mu\text{s}$.

statistics by running every configuration of parameters N_R times. The main observable we are interested in is the number of lasing modes, where a lasing mode is defined as any mode that has power $p_{\eta,i} \geq \epsilon p_0$, where p_0 is the steady-state power of a single oscillator [32]. We let the system run for a time t_{end} and choose $\epsilon = 0.9$ to account for the fluctuations around the equilibrium power of a STO. Our stochastic simulations may not capture all possible processes, such as rare low probability events, in a single run. However, by running multiple “trajectories” we can gather statistics and gain insight into the behavior of the system. This is also true of experimental runs, where the number of lasing modes will vary in any one realization of the experiment. We will discuss this problem in greater detail in Sec. IV B, where we also show how the experimental observation times should be chosen.

IV. RESULTS

In this section, we present the results from the simulations described in Sec. III. Unless stated otherwise, we set $\alpha = 10^{-2}$, $\omega/4\pi\gamma M = 0.5$, $J_{s,A} = 2\alpha\omega$, $J_{s,B} = 0$, and $G = \Omega_d = 0$, such that we are in the \mathcal{PT} -symmetric regime and work with an array of $N = 10$ unit cells. We run the simulations of Eqs. (1)–(3) for $4\pi\gamma M t = 10^5$, which for a typical STO with $4\pi\gamma M = 10$ GHz corresponds to $10 \mu\text{s}$ and collect statistics over $N_R = 100$ runs. We are interested in two main observables: whether the edge mode starts lasing, and how many bulk modes also start lasing. It is worth noting that since the B-sites dynamics are suppressed because they are not directly driven, we only have N possible lasing modes. We choose $k_B T/\lambda$ in the range 10^{-6} to 10^{-4} , with the latter corresponding to room temperature for a typical STO [32].

In Fig. 2 we show three typical examples of the system dynamics. The system is initially in thermal equilibrium, and at $t = 0$ the spin-torque current is turned on for all A sites. Figure 2(a) show the case where after some time the left-most mode starts lasing at the steady-state power for a single oscillator, whilst the dynamics of the bulk modes are suppressed. Alternatively, no modes can start lasing at all [Fig. 2(b)], which we will discuss further in Sec. IV B. We also observed the lasing of bulk modes together with the edge mode, as shown in Fig. 2(c). In this specific example the bulk mode starts lasing shortly after the edge mode. We have not

investigated this timing further, but it seems likely that a lasing edge mode could also excite bulk modes close to the edge. Moreover, we also observed cases where bulk modes start lasing later in time, seemingly independent of the lasing of the edge mode.

Since all three cases are possible, we further explore the parameter space, and focus on the amount of lasing modes as an observable. We note that in all of the cases discussed here we never observed a lasing bulk mode without a lasing edge mode. This is a direct result of the topology of the array.

As discussed before, the system hosts a lasing topological edge state for $-1 < J/|\tilde{J}| < 1$. We thus show the average number of lasing bulk (dashed line) and edge (solid line) modes as a function of $J/|\tilde{J}|$ for different temperatures in Fig. 3. The transition from the topological to the trivial regime at $J/|\tilde{J}| = -1$ is affected by the temperature. For low temperatures the transition is sharper than for high temperatures. However, at high temperatures the system still exhibits signs of a non-Hermitian topological insulator (suppressing of the bulk modes, with only a single lasing edge mode), even if the system is in the trivial phase, i.e., if $|J| > |\tilde{J}|$.

As was previously discussed, the system has broken \mathcal{PT} symmetry when $|\tilde{J} - \alpha\omega| < |J| < |\tilde{J} + \alpha\omega|$, where

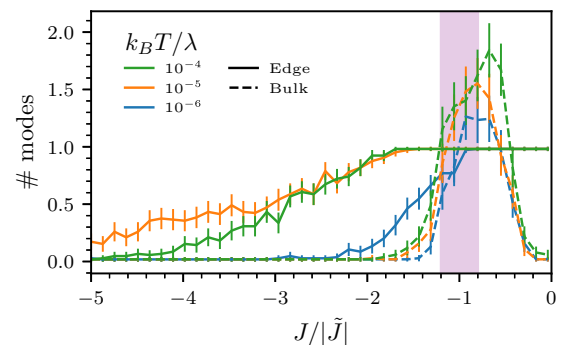


FIG. 3. Average number of lasing bulk (dashed line) and edge (solid line) modes as a function of $|J|$, for different temperatures. The \mathcal{PT} -broken regime is indicated by the shaded region. Note that these simulations were only run for $4\pi\gamma M t = 10^5$ and this is therefore only a snapshot of the number of lasing modes. The error bars show the 95% confidence interval.

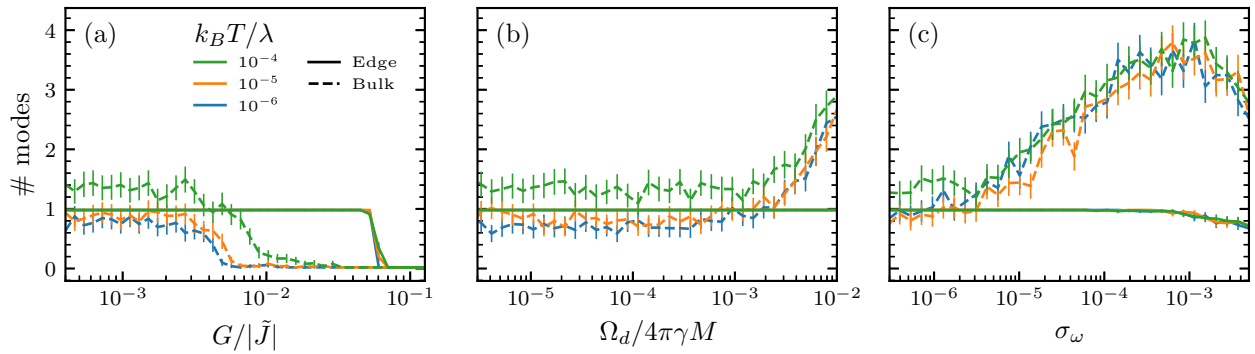


FIG. 4. Average number of lasing bulk (dashed line) and edge (solid line) modes for different perturbations that will always be present in any realistic system. The error bars show the 95% confidence interval. Here $\tilde{J} = -0.025/4\pi\gamma M$, $J/\tilde{J} = 0.5$. (a) As a function of the strength of the dissipative coupling $G = G_i = \tilde{G}_i$, which is mediated by the spacer layers between the STOs. (b) As a function of the dipole-dipole coupling strength $\Omega_d/4\pi\gamma M$, which can be tuned by the spacing between the STOs. (c) As function of the variation of the individual FMR-frequency $\omega_{\eta,i}$, chosen from a normal distribution with mean $\omega/4\pi\gamma M = 0.5$ and standard deviation σ_ω .

multiple modes will start to lase. In Fig. 3 the \mathcal{PT} -broken regime is indicated by the shaded area and it is easy to see that more bulk modes start lasing. For higher temperatures more bulk modes will start to lase. We remark here that these simulations were only run for a fixed time t_{end} , and therefore not all modes might have started lasing yet. We return to this issue in Sec. IV B.

The number of lasing bulk modes also increases as a function of temperature. Instead of a sharp transition at the exceptional point (EP), there is a transitional regime, due to the nonlinear and stochastic effects. This indicates that, depending on the operating temperature, it is necessary to stay further away from the EP than one might initially expect. Specifically for this parameter set it would mean choosing $|J| \ll |\tilde{J} + \alpha\omega|$, such that there are no unwanted bulk contributions from the \mathcal{PT} -broken regime. The fact that the \mathcal{PT} -broken regime extends further than expected might also have implications for applications using the exceptional point, such as enhanced sensing [49,50] and encircling the exceptional point [51].

A. Sensitivity to perturbations

We now consider three main perturbations present in any experimental realization of the system: (1) the dissipative coupling modulated by spin-waves traveling in the metallic spacer layer, (2) the dipole-dipole coupling between the macrospins of the STOs, and (3) variations in the parameters of the individual STOs.

We first consider the inter (intra)-layer dissipative coupling G (\tilde{G}), induced by the metallic spacer layer. This coupling is known to synchronize STOs [43]. Since it is modulated by the metallic spacer layer it can be tuned to an extent, e.g., by choosing a spacer layer with a certain spin relaxation. It is also possible to choose a STO nanopillar geometry in which the metallic spacer layer does not extend in between the STOs and therefore no spin waves can propagate, thus suppressing the dissipative coupling [32].

We vary the dissipative coupling $G = G_i = \tilde{G}_i$, the results of which are shown in Fig. 4(a). We note here that even though the dissipative coupling breaks the \mathcal{PT} symmetry, the edge modes are still protected by CI symmetry. When

$G/|\tilde{J}| > 10^{-3}$, first the bulk modes are suppressed. This can be attributed to the increased overall dissipation in the system, suppressing the bulk excitations. When $G/|\tilde{J}| > 0.05$ the edge modes are also suppressed, which again can be attributed to the increased overall dissipation. This result thus suggests that it is desirable to design a system where the dissipative coupling is weak, such as by using the nanopillar geometry. However, a small dissipative coupling might be beneficial, effectively suppressing the bulk excitations, while allowing the edge modes to lase.

Next, we discuss the dipole-dipole coupling, which is present in any magnetic system. It has also been known to synchronize the precession in STOs [43]. The dipolar coupling strength can be controlled by the spacing between the STOs. We vary the dipolar coupling strength $\Omega_d/4\pi\gamma M$ for different temperatures, as shown in Fig. 4(b). For small Ω_d we see no changes, and only for $\Omega_d/4\pi\gamma M > 10^{-3}$ the bulk modes will start to lase. For STOs of typical dimensions $10 \times 10 \times 10$ nm and a separation distance 10 nm, $\Omega_d/4\pi\gamma M \approx 10^{-3}$. Our results indicate a lower bound on the spacing between STOs in order to avoid activation of the bulk lasing modes due to the dipole-dipole interaction.

In any experimental setup there will be small variations between the individual STOs. Since the system considered here is only symmetric if the dissipation is balanced with the driving, even small variations in any parts of the STO array involved in the driving and dissipation processes will break the \mathcal{PT} symmetry. Since the topological classification of this system is based on the \mathcal{PT} symmetry, it is useful to consider the effect of breaking this symmetry.

In order to model spatial disorder we consider an array with small variations in the individual frequencies ω_i , by assuming they are normally distributed with standard deviation σ_ω and mean ω . If the local spin-transfer torque is kept constant at $J_s = 2\alpha\omega$ throughout the array, the system is no longer \mathcal{PT} symmetric. This spin-injection model corresponds to setup in which a single current source, rather than individual ones, are used to inject spin angular momentum into the STOs. The number of lasing modes is shown in Fig. 4(c), where it is clear that as the variance is increased, more bulk modes start lasing. The disorder we introduce

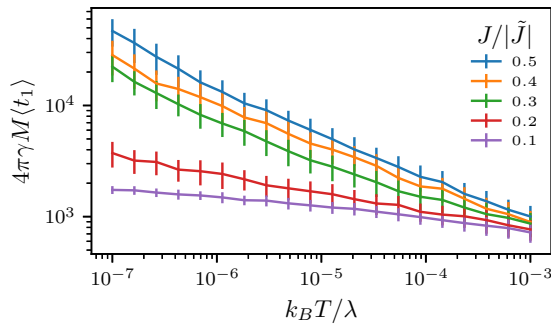


FIG. 5. The average time for the edge mode to start lasing, for different ratios $J/|\tilde{J}|$. These simulations are all in the unbroken \mathcal{PT} -regime. For a typical FMR frequency $4\pi\gamma M = 10$ GHz these times are in the order of 0.01 ms to 1 ms. The error bars show one standard deviation.

breaks the \mathcal{PT} symmetry, and the edge states are no longer topologically protected. The bulk modes are therefore no longer suppressed and can start lasing. We have also modeled the case where $J_{s,i} = 2\alpha\omega_i$, i.e., where the STOs are individually driven. This did not affect the results, indicating that it is not just the \mathcal{PT} symmetry within one unit cell, but rather the \mathcal{PT} symmetry of the complete array that protects the edge states. The robustness of non-Hermitian topological states against disorder is still poorly understood. From the linear dynamics we know that if a variance σ_ω is introduced the bulk modes also gain a nonzero imaginary component and will therefore start lasing or be suppressed. This is thus in essence not a nonlinear or stochastic effect, in contrast to the other effects discussed previously.

We thus conclude that the non-Hermitian SSH chain can be experimentally realized using STOs, but care needs to be taken to control the dissipative coupling, dipolar interactions and the variations between STOs.

B. Nucleation

The processes that we consider in this paper are fully stochastic, and so is the lasing of the edge mode: there is a finite probability that the edge mode will start lasing. It is therefore possible that even in the topological phase, the edge mode might only start lasing at time scales longer than the experimental observation time. Motivated by this consideration, we thus investigate here the nucleation times of the lasing edge modes.

As before, we prepare our system in thermal equilibrium, and turn on the spin current at $t = 0$. We only consider the RKKY-type coupling, and set $G = \tilde{G} = \Omega_d = 0$. In Fig. 5 we show the temperature dependence of the time at which the edge mode starts lasing, for different ratios $J/|\tilde{J}|$. We have chosen the ratio $J/|\tilde{J}|$ such that we are in the unbroken \mathcal{PT} regime and we only expect the edge state to start lasing.

It is clear that the time until the edge mode starts lasing follows an exponential distribution as a function of temperature. Moreover, for lower intracell coupling J , the average time decreases. This observation can be explained in terms of overcoming an energy barrier. The probability of the edge

mode to start lasing is

$$P_1 \propto \exp\left[-\frac{\Delta E}{k_B T}\right], \quad (8)$$

where ΔE is the energy difference between the state with no modes lasing and the state with a lasing edge mode, which is directly related to the coupling strength J .

The nucleation problem also illustrates that the finite runtimes inherent with numerical simulations might not be representative of experiments. Since the nucleation is a stochastic process, it is possible that for longer runtimes, such as seconds, all modes will start lasing. In order to have robust isolated edge modes, these devices might therefore be limited to shorter runtimes (on the order of μ s), especially at higher temperatures. The opposite problem of course also exist, where one has to wait a long time for the edge mode to start lasing. The nucleation time can however be tuned with the exchange coupling, as is shown in Fig. 5. The inherent stochastic nature of this device could make it useful for stochastic computing, which relies on systems with inherent randomness [52,53].

V. COMPARISON TO PHOTONIC SYSTEMS

The array of STOs considered here shares many similarities with the photonic microring resonators experimentally realized in Ref. [14]. The linear dynamics of the magnetic excitations considered in this model are closely related to the dynamics of the photonic excitations in the microring resonators. Both models realize the non-Hermitian SSH model as described by Eq. (4). Moreover, their nonlinear dynamics are similar, as we show next.

The dynamics of the microring resonator array are, up to second order in the (normalized) electric modal field amplitudes a_n^η , described by [54]

$$\begin{aligned} \partial_t a_n^A &= -i\Omega a_n^A - \gamma - \sigma_A(1 - |a_n^A|^2) \\ &\quad + i\kappa_1 a_n^B + i\kappa_2 a_{n-1}^B, \\ \partial_t a_n^B &= -i\Omega a_n^B - \gamma - \sigma_B(1 - |a_n^B|^2) \\ &\quad + i\kappa_1 a_n^A + i\kappa_2 a_{n+1}^A, \end{aligned} \quad (9)$$

where Ω is the lasing mode frequency, γ is the mode loss, σ_η is the mode gain, and $\kappa_{1,2}$ are the coupling constants. Thus, we can draw a direct analog between the two systems, by identifying γ as the constant part of the Gilbert damping ($\gamma = \alpha\omega$), the lasing mode frequency Ω as the precession frequency ($\Omega = \omega$) and the mode gain as the spin current contribution ($\sigma_\eta = J_{s,\eta}$). One distinction is the linear coupling $\kappa_{1,2}$, whereas the RKKY coupling between the STOs is nonlinear. However, we note that up to first order in p_i the RKKY coupling is linear as well. In order to fully describe the dynamics of the microring resonators the carrier density also has to be taken into account. However, for timescales longer than the time-response of the laser, typically a few nanoseconds [55], the carrier dynamics can be disregarded and one obtains Eq. (9).

Most importantly, both systems have saturated gain. This feature is inherent to many driven non-Hermitian system, if the driving is limited in some way. We do note that the

nonlinear contributions to the precession and Gilbert damping that are present in STO systems are not present in photonics. The phase diagram, as presented in Fig. 3, might thus be different for the photonic system.

In this paper we have considered three perturbations: dissipative couplings, dipole-dipole interactions, and variations in the FMR-frequency, as shown in Fig. 4. Dissipative coupling can also be present in photonic systems, but when employing evanescent coupling is usually negligible [56], indicating that it is less relevant for photonic implementations of the non-Hermitian SSH chain. The long-range dipole-dipole interaction has no photonic analog, but variations in the parameters are inevitably present in photonic systems.

Nonlinear effects are a common feature of many experimental realizations of non-Hermitian systems. Our results are therefore applicable beyond STO arrays to other non-Hermitian topological phases.

VI. CONCLUSIONS AND DISCUSSIONS

In conclusion, we have shown that the lasing topological edge states can be successfully accessed using STOs in a realistic non-Hermitian SSH array. We have considered both nonlinear and stochastic dynamics, to determine if an experimental implementation of this model is feasible. Firstly, we found that the lasing edge mode is robust in the presence of a wide range of temperatures and perturbations, provided that we are in the topological regime. This occurs despite various perturbations breaking the \mathcal{PT} symmetry of the original Hamiltonian such that topological protection is not guaranteed. Our result is important for ensuring that the lasing edge mode can be probed in an experiment. Secondly, we found that even though the system is topological in the linear regime, in which no bulk modes should start to lase, nonlinear and stochastic effects can still access these bulk modes, reducing the usefulness of the topologically protected edge modes. We have explored the transition between the \mathcal{PT} -unbroken and \mathcal{PT} -broken regimes, which is not a sharp transition. Instead, we find a regime around the exceptional point where more bulk modes will start to lase.

Moreover, we have considered three kinds of perturbations that can naturally be present in this array and have shown in which regime the topology of the system is unaffected. We hope that these results can be used to guide future experiments. We find that at a given temperature and for equal strength of the perturbative term, the perturbation that mostly affects the dynamics of bulk modes is the variation in the parameters of the individual STOs. This might complicate the experimental realization of the STO array, and will be an inherent complication in any physical realization of a non-Hermitian SSH model, where variations are more likely. Finally, we have shown that there is a finite nucleation time, after which the edge state will start lasing.

Interactions between STOs as considered here are not easily tunable, since they depend on the spacing between the STOs [43]. Moreover, STOs cannot be brought arbitrarily close together because of Joule heating [57]. To circumvent this problem, one could couple the STOs using strip-line antennas above each STO, controlled by the microwave current generated at the adjacent STO [58]. This more direct

method has the advantage that the signal could be electrically amplified, thus allowing control over the coupling strength. Even though this coupling has a different physical origin, the conclusions as presented in this paper will still hold.

ACKNOWLEDGMENTS

R.D. is member of the D-ITP consortium, a program of the Dutch Organization for Scientific Research (NWO) that is funded by the Dutch Ministry of Education, Culture and Science (OCW). This project has received funding from the European Research Council (ERC) under the European Union's Horizon 2020 research and innovation programme (Grant Agreement No. 725509). This work is part of the research programme of the Foundation for Fundamental Research on Matter (FOM), which is part of the Netherlands Organization for Scientific Research (NWO). This work is part of the Fluid Spintronics research programme with Project No. 182.069, which is financed by the Dutch Research Council (NWO) B.F. acknowledges support of the National Science Foundation under Grant No. NSF DMR-2144086.

APPENDIX A: NUMERICAL IMPLEMENTATION

A single STO η in unit cell i can be parametrized with the complex amplitude $c_{\eta,i}(t)$ [32]

$$\mathbf{m}_{\eta,i} = M_{\eta,i} \begin{pmatrix} \sqrt{1 - p_{\eta,i}}(c_{\eta,i} + c_{\eta,i}^*) \\ \sqrt{1 - p_{\eta,i}}(ic_{\eta,i} - ic_{\eta,i}^*) \\ 1 - 2p_{\eta,i} \end{pmatrix}, \quad (\text{A1})$$

where $p_{\eta,i} = |c_{\eta,i}|^2$ and $M_{\eta,i}$ is the magnetization length. The Langevin equation of motion then becomes

$$\begin{aligned} \frac{dc_{\eta,i}}{dt} + i\omega_{\eta,i}(p_{\eta,i})c_{\eta,i} + \Gamma_{\eta,i}^+(p_{\eta,i})c_{\eta,i} \\ - \Gamma_{\eta,i}^-(p_{\eta,i})c_{\eta,i} = f_{\eta,i}(t), \end{aligned} \quad (\text{A2})$$

where

$$\omega_{\eta,i}(p) = \omega + 2p, \quad (\text{A3})$$

$$\Gamma_{\eta,i}^+(p) = \omega_{\eta,i}\alpha_{\eta,i}(1 + (2/\omega_{\eta,i} - 1)p), \quad (\text{A4})$$

$$\Gamma_{\eta,i}^-(p) = J_{s;\eta,i}(1 - p), \quad (\text{A5})$$

where the superscript $+$ ($-$) indicates loss (gain) and $f_{\eta,i}(t)$ is a complex field, representing the thermal fluctuations. The stochastic field is a phenomenological description of all thermal processes and chosen to have zero mean and a second-order correlator

$$\begin{aligned} \langle f_{\eta,i}(t)f_{\eta',j}(t') \rangle &= 0, \quad \langle f_{\eta,i}(t)f_{\eta',j}^*(t') \rangle \\ &= 2\delta_{i,j}\delta_{\eta,\eta'}D_{\eta,i}(p_{\eta,i})\delta(t - t'), \end{aligned} \quad (\text{A6})$$

The diffusion coefficient $D_{\eta,i}(p)$ has to be taken dependent on p such that the system tends to thermal equilibrium. This is done by deriving the Fokker-Planck equation from the Langevin Eq. (A2) and finding a physically-consistent solution [38]. For a single STO this is

$$D_{\eta,i}(p) = \Gamma_{\eta,i}^+(p) \frac{k_B T}{\lambda_{\eta,i}\omega_{\eta,i}(p)}, \quad (\text{A7})$$

where $\lambda_{\eta,i}$ is a scale factor relating the dimensionless oscillator power p and the oscillator energy, which is $\lambda_{\eta,i} = V_{\text{eff}\eta,i} M_{\eta,i} / \gamma_{\eta,i}$ for our choice of parametrization.

As initial conditions we choose $c_{\eta,i} = \sqrt{p_0} e^{i\phi}$, where ϕ is randomly chosen between 0 and 2π and p_0 is drawn from a thermal equilibrium distribution P_{eq} for an ensemble of isolated STOs

$$P_{\text{eq}} \propto \exp \left[-\frac{2\lambda_{\eta,i}}{k_B T} p_{\eta,i} \right]. \quad (\text{A8})$$

For the array as considered in the main text, the equation of motion is given by

$$\begin{aligned} \partial_t c_{A,i} &= f_{\text{STO}}(c_{A,i}) c_{A,i} \\ &+ J_i f_J(c_{A,i}, c_{B,i}) + \tilde{J}_{i-1} f_J(c_{A,i}, c_{i-1,B}) \end{aligned}$$

$$\begin{aligned} &+ G_i f_G(c_{A,i}, c_{B,i}) + \tilde{G}_{i-1} f_G(c_{A,i}, c_{i-1,B}) \\ &+ \Omega_d \sum'_{\eta,j} \frac{f_{\text{dip}}(c_{A,i}, c_{j,\eta})}{r_{Ai,\eta j}^3}, \end{aligned} \quad (\text{A9})$$

$$\begin{aligned} \partial_t c_{B,i} &= f_{\text{STO}}(c_{B,i}) c_{B,i} \\ &+ J_i f_J(c_{B,i}, c_{A,i}) + \tilde{J}_i f_J(c_{B,i}, c_{i+1,A}) \\ &+ G_i f_G(c_{B,i}, c_{A,i}) + \tilde{G}_{i-1} f_G(c_{B,i}, c_{i+1,A}), \\ &+ \Omega_d \sum'_{\eta,j} \frac{f_{\text{dip}}(c_{B,i}, c_{j,\eta})}{r_{Bi,\eta j}^3}, \end{aligned} \quad (\text{A10})$$

where $f_J(c_{\eta,i}, c_{j,\eta'})$, $f_G(c_{\eta,i}, c_{j,\eta'})$ and $f_{\text{dip}}(c_{B,i}, c_{j,\eta})$ are the RRY, dissipative and dipolar couplings between the $\text{STO}_{\eta i}$ and $\text{STO}_{\eta' j}$. These are given by

$$f_{\text{STO}}(c_{\eta,i}) = -i(\omega_{\eta,i} + 2p_{\eta,i}) - \alpha_{\eta,i} \omega_{\eta,i} (1 + (2/\omega_{\eta,i} - 1)p_{\eta,i}) + J_{s,\eta,i} (1 - p_{\eta,i}), \quad (\text{A11})$$

$$f_J(c_{\eta,i}, c_{j,\eta'}) = \frac{i}{2\sqrt{1-p_{\eta,i}}} (c_{j,\eta'} (2 - 3p_{\eta,i}) \sqrt{1-p_{j,\eta'}} + c_{\eta,i} c_{j,\eta'}^* (4c_{j,\eta'} \sqrt{1-p_{\eta,i}} - c_{\eta,i} \sqrt{1-p_{j,\eta'}}) - 2c_{\eta,i} \sqrt{1-p_{\eta,i}}), \quad (\text{A12})$$

$$\begin{aligned} f_G(c_{\eta,i}, c_{j,\eta'}) &= \frac{1}{1-p_{\eta,i}} (c_{j,\eta'} \omega_{j,\eta'} (-\sqrt{1-p_{j,\eta'}} \sqrt{1-p_{\eta,i}} + c_{j,\eta'}^* (2c_{j,\eta'} \sqrt{1-p_{j,\eta'}} \sqrt{1-p_{\eta,i}} - c_{\eta,i})) \\ &- 2c_{j,\eta'} p_{j,\eta'} (\sqrt{1-p_{j,\eta'}} \sqrt{1-p_{\eta,i}} + c_{\eta,i} c_{j,\eta'}^*)), \end{aligned} \quad (\text{A13})$$

$$\begin{aligned} f_{\text{dip}}(c_{\eta,i}, c_{j,\eta'}) &= \frac{i}{\sqrt{1-p_{\eta,i}}} (c_{\eta,i} \sqrt{1-p_{\eta,i}} + 2c_{\eta,i}^2 c_{j,\eta'}^* \sqrt{1-p_{j,\eta'}} - 2c_{\eta,i} p_{j,\eta'} \sqrt{1-p_{\eta,i}} \\ &- \sqrt{1-p_{j,\eta'}} (1 - 3c_{\eta,i} \text{Re}[c_{\eta,i}]) (c_{j,\eta'} - 3\text{Re}[c_{j,\eta'}])). \end{aligned} \quad (\text{A14})$$

APPENDIX B: HAMILTONIAN

The full Hamiltonian is given by $H = \sum_i H_i + H_i^G + H_i^{\text{dip}}$, where H_i is given in Eq. (4) and

$$H_i^G = iG\omega[a_i^\dagger b_i + \text{H.c.}] + i\tilde{G}\omega[a_i^\dagger b_{i-1} + \text{H.c.}], \quad (\text{B1})$$

$$H_i^{\text{dip}} = \Omega_d \sum_{\eta} \left[\eta_i^\dagger \eta_i + \sum'_{j,\eta'} \frac{\eta_i^\dagger \eta'_j + 3\eta_i^\dagger \eta'_j + 3\eta_i \eta'_j}{2r_{\eta i, \eta' j}^3} \right], \quad (\text{B2})$$

with $\eta, \eta' = a, b$ and the \sum' indicates that the sum excludes self-interactions (i.e., $i = j, \nu = \eta$). The boundary conditions are then given by Eq. (5) and

$$H_j^G = iG\omega[a_j^\dagger b_j + \text{H.c.}] + i\tilde{G}\omega[b_j^\dagger a_l + \text{H.c.}]. \quad (\text{B3})$$

- [1] M. Z. Hasan and C. L. Kane, Colloquium: Topological insulators, *Rev. Mod. Phys.* **82**, 3045 (2010).
- [2] C. M. Bender, D. C. Brody, and H. F. Jones, Complex Extension of Quantum Mechanics, *Phys. Rev. Lett.* **89**, 270401 (2002).
- [3] C. M. Bender and S. Boettcher, Real Spectra in Non-Hermitian Hamiltonians Having \mathcal{PT} Symmetry, *Phys. Rev. Lett.* **80**, 5243 (1998).
- [4] E. J. Bergholtz, J. C. Budich, and F. K. Kunst, Exceptional topology of non-Hermitian systems, *Rev. Mod. Phys.* **93**, 015005 (2021).

- [5] K. Kawabata, K. Shiozaki, M. Ueda, and M. Sato, Symmetry and Topology in Non-Hermitian Physics, *Phys. Rev. X* **9**, 041015 (2019).
- [6] Z. Gong, Y. Ashida, K. Kawabata, K. Takasan, S. Higashikawa, and M. Ueda, Topological Phases of Non-Hermitian Systems, *Phys. Rev. X* **8**, 031079 (2018).
- [7] H. Shen, B. Zhen, and L. Fu, Topological Band Theory for Non-Hermitian Hamiltonians, *Phys. Rev. Lett.* **120**, 146402 (2018).
- [8] C.-K. Chiu, J. C. Y. Teo, A. P. Schnyder, and S. Ryu, Classification of topological quantum matter with symmetries, *Rev. Mod. Phys.* **88**, 035005 (2016).

- [9] K. Kawabata, K. Shiozaki, and M. Ueda, Anomalous helical edge states in a non-Hermitian Chern insulator, *Phys. Rev. B* **98**, 165148 (2018).
- [10] V. M. Martínez Alvarez, J. E. Barrios Vargas, and L. E. F. Foa Torres, Non-Hermitian robust edge states in one dimension: Anomalous localization and eigenspace condensation at exceptional points, *Phys. Rev. B* **97**, 121401(R) (2018).
- [11] D. S. Borgnia, A. J. Kruchkov, and R.-J. Slager, Non-Hermitian Boundary Modes and Topology, *Phys. Rev. Lett.* **124**, 056802 (2020).
- [12] S. Yao and Z. Wang, Edge States and Topological Invariants of Non-Hermitian Systems, *Phys. Rev. Lett.* **121**, 086803 (2018).
- [13] F. K. Kunst, E. Edvardsson, J. C. Budich, and E. J. Bergholtz, Biorthogonal Bulk-Boundary Correspondence in Non-Hermitian Systems, *Phys. Rev. Lett.* **121**, 026808 (2018).
- [14] M. Parto, S. Wittek, H. Hodaei, G. Harari, M. A. Bandres, J. Ren, M. C. Rechtsman, M. Segev, D. N. Christodoulides, and M. Khajavikhan, Edge-Mode Lasing in 1D Topological Active Arrays, *Phys. Rev. Lett.* **120**, 113901 (2018).
- [15] M. A. Bandres, S. Wittek, G. Harari, M. Parto, J. Ren, M. Segev, D. N. Christodoulides, and M. Khajavikhan, Topological insulator laser: Experiments, *Science* **359**, eaar4005 (2018).
- [16] G. Harari, M. A. Bandres, Y. Lumer, M. C. Rechtsman, Y. D. Chong, M. Khajavikhan, D. N. Christodoulides, and M. Segev, Topological insulator laser: Theory, *Science* **359**, eaar4003 (2018).
- [17] V. V. Albert, L. I. Glazman, and L. Jiang, Topological Properties of Linear Circuit Lattices, *Phys. Rev. Lett.* **114**, 173902 (2015).
- [18] M. Ezawa, Non-Hermitian higher-order topological states in nonreciprocal and reciprocal systems with their electric-circuit realization, *Phys. Rev. B* **99**, 201411(R) (2019).
- [19] S. Liu, S. Ma, C. Yang, L. Zhang, W. Gao, Y. J. Xiang, T. J. Cui, and S. Zhang, Gain- and Loss-Induced Topological Insulating Phase in a Non-Hermitian Electrical Circuit, *Phys. Rev. Appl.* **13**, 014047 (2020).
- [20] H. Zhao, P. Miao, M. H. Teimourpour, S. Malzard, R. El-Ganainy, H. Schomerus, and L. Feng, Topological hybrid silicon microlasers, *Nat. Commun.* **9**, 981 (2018).
- [21] T. Ozawa, H. M. Price, A. Amo, N. Goldman, M. Hafezi, L. Lu, M. C. Rechtsman, D. Schuster, J. Simon, O. Zilberberg, and I. Carusotto, Topological photonics, *Rev. Mod. Phys.* **91**, 015006 (2019).
- [22] V. M. Martínez Alvarez, J. E. Barrios Vargas, M. Berdakin, and L. E. F. Foa Torres, Topological states of non-Hermitian systems, *Eur. Phys. J.: Spec. Top.* **227**, 1295 (2018).
- [23] Ş. K. Özdemir, S. Rotter, F. Nori, and L. Yang, Parity–time symmetry and exceptional points in photonics, *Nat. Mater.* **18**, 783 (2019).
- [24] R. Su, E. Estrecho, D. Biegańska, Y. Huang, M. Wurdack, M. Pieczarka, A. G. Truscott, T. C. H. Liew, E. A. Ostrovskaya, and Q. Xiong, Direct measurement of a non-Hermitian topological invariant in a hybrid light-matter system, *Sci. Adv.* **7**, eabj8905 (2021).
- [25] A. Ghatak, M. Brandenbourger, J. van Wezel, and C. Coulais, Observation of non-Hermitian topology and its bulk–edge correspondence in an active mechanical metamaterial, *Proc. Natl. Acad. Sci. USA* **117**, 29561 (2020).
- [26] C. Scheibner, W. T. M. Irvine, and V. Vitelli, Non-Hermitian Band Topology and Skin Modes in Active Elastic Media, *Phys. Rev. Lett.* **125**, 118001 (2020).
- [27] T. Helbig, T. Hofmann, S. Imhof, M. Abdelghany, T. Kiessling, L. W. Molenkamp, C. H. Lee, A. Szameit, M. Greiter, and R. Thomale, Generalized bulk–boundary correspondence in non-Hermitian topoelectrical circuits, *Nat. Phys.* **16**, 747 (2020).
- [28] J. M. Lee, T. Kottos, and B. Shapiro, Macroscopic magnetic structures with balanced gain and loss, *Phys. Rev. B* **91**, 094416 (2015).
- [29] P. A. McClarty and J. G. Rau, Non-Hermitian topology of spontaneous magnon decay, *Phys. Rev. B* **100**, 100405(R) (2019).
- [30] K. Deng and B. Flebus, Non-Hermitian skin effect in magnetic systems, [arXiv:2109.01711](https://arxiv.org/abs/2109.01711)
- [31] B. Flebus, R. A. Duine, and H. M. Hurst, Non-Hermitian topology of one-dimensional spin-torque oscillator arrays, *Phys. Rev. B* **102**, 180408(R) (2020).
- [32] A. Slavin and V. Tiberkevich, Nonlinear auto-oscillator theory of microwave generation by spin-polarized current, *IEEE Trans. Magn.* **45**, 1875 (2009).
- [33] S. Kaka, M. R. Pufall, W. H. Rippard, T. J. Silva, S. E. Russek, and J. A. Katine, Mutual phase-locking of microwave spin torque nano-oscillators, *Nature (London)* **437**, 389 (2005).
- [34] F. B. Mancoff, N. D. Rizzo, B. N. Engel, and S. Tehrani, Phase-locking in double-point-contact spin-transfer devices, *Nature (London)* **437**, 393 (2005).
- [35] W. P. Su, J. R. Schrieffer, and A. J. Heeger, Solitons in Polyacetylene, *Phys. Rev. Lett.* **42**, 1698 (1979).
- [36] S. Lieu, Topological phases in the non-Hermitian Su-Schrieffer-Heeger model, *Phys. Rev. B* **97**, 045106 (2018).
- [37] K. Yokomizo and S. Murakami, Non-Bloch Band Theory of Non-Hermitian Systems, *Phys. Rev. Lett.* **123**, 066404 (2019).
- [38] V. Tiberkevich, A. Slavin, and J.-V. Kim, Microwave power generated by a spin-torque oscillator in the presence of noise, *Appl. Phys. Lett.* **91**, 192506 (2007).
- [39] A. Houshang, E. Iacocca, P. Dürrenfeld, S. R. Sani, J. Åkerman, and R. K. Dumas, Spin-wave-beam driven synchronization of nanocontact spin-torque oscillators, *Nat. Nanotechnol.* **11**, 280 (2016).
- [40] N. Locatelli, A. Hamadeh, F. Abreu Araujo, A. D. Belanovsky, P. N. Skirdkov, R. Lebrun, V. V. Naletov, K. A. Zvezdin, M. Muñoz, J. Grollier, O. Klein, V. Cros, and G. de Loubens, Efficient synchronization of dipolarly coupled vortex-based spin transfer nano-oscillators, *Sci. Rep.* **5**, 17039 (2015).
- [41] M. Ezawa, Nonlinearity-induced transition in the nonlinear Su-Schrieffer-Heeger model and a nonlinear higher-order topological system, *Phys. Rev. B* **104**, 235420 (2021).
- [42] M. Ezawa, Nonlinear non-Hermitian higher-order topological laser, *Phys. Rev. Research* **4**, 013195 (2022).
- [43] A. N. Slavin and V. S. Tiberkevich, Theory of mutual phase locking of spin-torque nanosized oscillators, *Phys. Rev. B* **74**, 104401 (2006).
- [44] T. Holstein and H. Primakoff, Field dependence of the intrinsic domain magnetization of a ferromagnet, *Phys. Rev.* **58**, 1098 (1940).
- [45] L. Jin and Z. Song, Bulk-boundary correspondence in a non-Hermitian system in one dimension with chiral inversion symmetry, *Phys. Rev. B* **99**, 081103(R) (2019).
- [46] Z.-X. Gong, M. F. Maghrebi, A. Hu, M. L. Wall, M. Foss-Feig, and A. V. Gorshkov, Topological phases with long-range interactions, *Phys. Rev. B* **93**, 041102(R) (2016).
- [47] J.-V. Kim, Q. Mistral, C. Chappert, V. S. Tiberkevich, and A. N. Slavin, Line Shape Distortion in a Nonlinear Auto-Oscillator

- Near Generation Threshold: Application to Spin-Torque Nano-Oscillators, *Phys. Rev. Lett.* **100**, 167201 (2008).
- [48] C. Rackauckas and Q. Nie, Differential equations.jl—A performant and feature-rich ecosystem for solving differential equations in julia, *J. Open Res. Softw.* **5**, 15 (2017).
- [49] W. Chen, Ş. Kaya Özdemir, G. Zhao, J. Wiersig, and L. Yang, Exceptional points enhance sensing in an optical microcavity, *Nature (London)* **548**, 192 (2017).
- [50] M.-A. Miri and A. Alù, Exceptional points in optics and photonics, *Science* **363**, eaar7709 (2019).
- [51] C. Dembowski, B. Dietz, H.-D. Gräf, H. L. Harney, A. Heine, W. D. Heiss, and A. Richter, Encircling an exceptional point, *Phys. Rev. E* **69**, 056216 (2004).
- [52] A. F. Vincent, J. Larroque, N. Locatelli, N. Ben Romdhane, O. Bichler, C. Gamrat, W. S. Zhao, J.-O. Klein, S. Galdin-Retailleau, and D. Querlioz, Spin-transfer torque magnetic memory as a stochastic memristive synapse for neuromorphic systems, *IEEE Trans. Biomed. Circuits Syst.* **9**, 166 (2015).
- [53] J. Grollier, D. Querlioz, K. Y. Camsari, K. Everschor-Sitte, S. Fukami, and M. D. Stiles, Neuromorphic spintronics, *Nat. Electron.* **3**, 360 (2020).
- [54] A. U. Hassan, H. Hodaei, M.-A. Miri, M. Khajavikhan, and D. N. Christodoulides, Nonlinear reversal of the \mathcal{PT} -symmetric phase transition in a system of coupled semiconductor microring resonators, *Phys. Rev. A* **92**, 063807 (2015).
- [55] G. P. Agrawal and N. K. Dutta, *Semiconductor Lasers* (Springer US, Boston, 1995).
- [56] J. Ding and M.-A. Miri, Mode discrimination in dissipatively coupled laser arrays, *Opt. Lett.* **44**, 5021 (2019).
- [57] A. Slavin, Spin-torque oscillators get in phase, *Nat. Nanotechnol.* **4**, 479 (2009).
- [58] S. Wittrock, S. Perna, R. Lebrun, R. Dutra, R. Ferreira, P. Bortolotti, C. Serpico, and V. Cros, Exceptional points controlling oscillation death in coupled spintronic nano-oscillators, [arXiv:2108.04804](https://arxiv.org/abs/2108.04804).